applied sciences

MDPI

Article

Left Ventricular Ejection Time Estimation from Blood Pressure and Photoplethysmography Signals Based on Tidal Wave

Lucian Evdochim [1,*], Dragoș Dobrescu [1], Lidia Dobrescu [1], Silviu Stanciu [2] and Stela Halichidis [3]

[1] Department of Electronic Devices, Circuits and Architectures, Faculty of Electronics, Telecommunications and Information Technology, University Politehnica of Bucharest, 060042 Bucharest, Romania
[2] Laboratory of Cardiovascular Noninvasive Investigations, Dr. Carol Davila Central Military Emergency University Hospital, 010825 Bucharest, Romania
[3] Department of Clinical Medical Disciplines, Faculty of Medicine, Ovidius University of Constanta, 900527 Constanta, Romania
* Correspondence: lucian.evdochim@stud.etti.upb.ro; Tel.: +00-407-2278-6181

Featured Application: Left ventricular ejection time estimation by analyzing the morphology of arterial blood pressure and photoplethysmography signal.

Abstract: Left ventricular ejection time (LVET) is an important parameter for assessing cardiovascular disorders. In a medical office, it is typically measured using the Tissue Doppler Imaging technique, but new wearable devices have led to a growing interest in integrating this parameter into them, increasing accessibility to personalized healthcare for users and patients. In the cardiovascular domain, photoplethysmography (PPG) is a promising technology that shares two distinctive features with invasive arterial blood pressure (ABP) tracing: the tidal wave (TDW) and the dicrotic wave (DCW). In the early years of cardiovascular research, the duration of the dicrotic point was initially linked to the ending phase of left ventricular ejection. Subsequent studies reported deviations from the initial association, suggesting that the ejection period is related to the tidal wave feature. In this current study, we measured left ventricular ejection time in both ABP and PPG waveforms, considering recent research results. A total of 27,000 cardiac cycles were analyzed for both afore-mentioned signals. The reference value for ejection time was computed based on the T-wave segment duration from the electrocardiogram waveform. In lower blood pressure, which is associated with decreased heart contractility, the results indicated an underestimation of -29 ± 19 ms in ABP and an overestimation of 18 ± 31 ms in PPG. On the other side of the spectrum, during increased contractility, the minimum errors were -3 ± 18 ms and 4 ± 33 ms, respectively. Since the tidal wave feature is strongly affected by arterial tree compliance, the population evaluation results indicate a Pearson's correlation factor of 0.58 in the ABP case, and 0.53 in PPG. These findings highlight the need for advanced compensation techniques, in particular for PPG assessment, to achieve clinical-grade accuracy.

Keywords: tidal wave; dicrotic wave; left ventricular ejection time; photoplethysmography; blood pressure; electrocardiogram; signal database

check for updates

Citation: Evdochim, L.; Dobrescu, D.; Dobrescu, L.; Stanciu, S.; Halichidis, S. Left Ventricular Ejection Time Estimation from Blood Pressure and Photoplethysmography Signals Based on Tidal Wave. *Appl. Sci.* **2023**, *13*, 11025. https://doi.org/10.3390/app131911025

Academic Editors: Bo Yang, Bo Jin and Xiaoyan Chen

Received: 31 August 2023
Revised: 4 October 2023
Accepted: 5 October 2023
Published: 6 October 2023

Copyright: © 2023 by the authors. Licensee MDPI, Basel, Switzerland. This article is an open access article distributed under the terms and conditions of the Creative Commons Attribution (CC BY) license (https://creativecommons.org/licenses/by/4.0/).

1. Introduction

Monitoring heart activity and its associated hemodynamic parameters plays a significant role in managing cardiovascular disorders (CVD). Dysfunction related to the heart muscle, aside from issues within the vessel network, encompasses conditions such as heart failure (HF), heart valve disease, arrhythmia and stroke [1–4]. One of the key cardiovascular markers is left ventricular ejection time (LVET or ET), which characterizes ventricular performance metrics, including contractility. It offers insights into the efficiency of the heart's pumping mechanism and can aid in the diagnosis and management of the afore-mentioned disorders. Moreover, being supported by additional markers such as isovolumetric contraction time (IVCT) and relaxation time (IVRT), it derives the Myocardial

Performance Index (MPI or TEI-index), a simple tool to identify cardiac dysfunction. In recent years, there has been growing interest in measuring this parameter for therapeutic purposes with novel drugs [2].

A significant advancement in personalized healthcare would involve making LVET assessment accessible through wearable technologies. Individuals could seamlessly integrate this parameter into their daily lives through portable devices aimed at hemodynamic monitoring. The continuous data stream would not only provide valuable insights into their cardiovascular health but also enable the early detection of abnormalities and timely intervention. The potential benefits in terms of preventing heart-related complications and improving overall well-being are immense. Also, due to the portability capabilities of wearable devices, cardiovascular performance could be monitored remotely, reducing the need for periodic visits to a medical office.

Over the last decade, wearable devices have gained significant traction in the healthcare domain by providing accurate readings, such as heart rate (HR) and blood oxygen saturation ratio SpO2 [5–7]. Photoplethysmography (PPG) is one of the most popular current technologies used in these devices, holding enormous potential in the field of hemodynamics. As a result, companies like Samsung have developed smartwatches with blood pressure (BP) estimation [8,9], although there are still challenges to overcome. Therefore, this capability is more addressable to the general market user rather than being primarily intended for clinical applications. Given that PPG waveform morphology closely resembles arterial blood pressure (ABP) tracing [10–13], it shares vital cardiovascular information. The most distinctive fiducial points along the signal contour are the tidal wave (TDW) and the dicrotic wave (DCW). However, advancements cannot be achieved without a proper interpretation of the waveform in synergy with human physiology and the associated deviations. The dicrotic wave feature has been reported since Wiegger's studies in the cardiovascular domain [14,15], where he published the first cardiac phase diagram, depicted in Figure 1a. This fiducial point has shown a strong link with vasomotor activity, especially during the action of therapeutic drugs [16–18]. Under vasopressor infusion, the dicrotic wave decreases in amplitude and moves toward the systolic point (SYS). Conversely, in the opposite effect, the point's location moves to the next diastolic valley (DIA) region at the same time with an amplitude amplification effect. Initially, this cardiovascular marker was also associated with the ending of the systolic phase, marked by LVET. However, during the development of medical signal processing, the correlation between DCW and ejection time was not thoroughly investigated. The technical limitations of the devices used to record cardiac events primarily consisted of two factors [19–21]. Firstly, the mechanical nature of the transducer used, such as manometers, had a reduced dynamic response due to fluid inertia, reducing the ability to record rapid changes during invasive arterial waveform tracing. Secondly, analog information could not be easily transferred digitally and processed. In the late 1950s, Wilkinson designed a feasible analog-to-digital converter (ADC), which accelerated developments in information technology [22]. Until this point, waveforms such as ABP or PPG had not fully harnessed the capabilities of digital signal processing techniques.

The other distinctive point, the tidal wave, was mentioned in the scientific community in the late 1980s. By revisiting Wiegger's diagram, this new feature became clearly evident on the waveform contour, appearing at a separate location from the classical dicrotic wave [23]. The development of Tissue Doppler Imaging (TDI) technology provided a more comprehensive understanding of heart mechanics [24–27]. Research in the cardiovascular domain, supported by the Doppler method, identified TDW as a more reliable predictor of LVET compared to the initially recognized DCW marker [28–30]. While ejection time was indirectly measured as the duration of the T-wave from an electrocardiogram (ECG) or obtained from the blood flow velocity profile using TDI, the results consistently matched fairly. An extensive analysis [31] demonstrated that for the precise conclusion of the ejection phase, the closure of the aortic valves must be considered, with a duration of 26 ± 16 ms. This information is critical to understanding the finite physiological phenomena in the

context of the TDW's origin. Currently, the proposed origin of this fiducial point is attributed to blood pressure wave reflection [32]. As result of the afore-mentioned findings, it is evident that the extraction of ejection time from the PPG signal is indeed feasible.

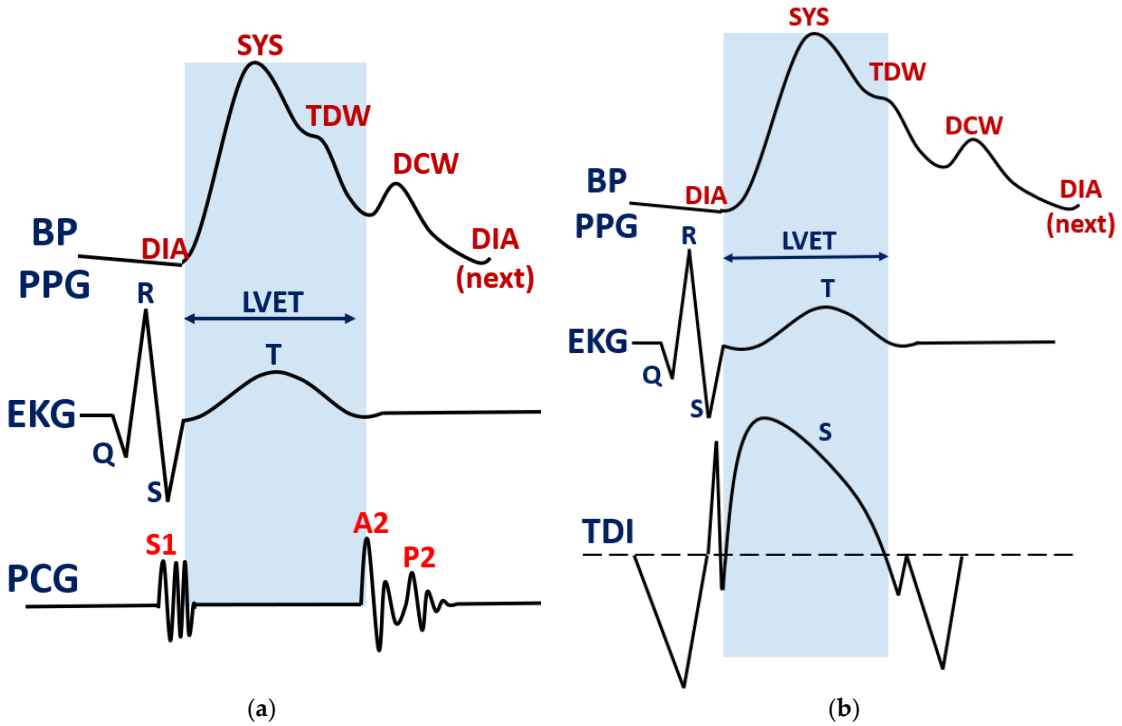


Figure 1. Correlation of ABP or PPG features with LVET. (**a**) First initial definition by Wiegger: ending of the ejection phase is marked by the dicrotic notch; (**b**) Updated correction following recent cardiovascular findings: ending of the ejection time is marked by the tidal wave, an earlier event compared to the notch.

In Figure 1, the correlation between LVET and fiducial points in ABP or PPG waveforms is illustrated, along with a corrected cardiac diagram resulting from the development of the TDI technique. Figure 1a shows Wieggers' synchronization of the ejection phase with heart sounds S1, A2 and P2, as obtained from a phonocardiogram (PCG). In Figure 1b, it is observed that LVET precedes the dicrotic notch in ABP or PPG, based on newer Doppler echography findings. Point S represents peak systolic myocardial velocity, a special marker for ejection phase assessment.

Therefore, in the context of the new findings, the tidal wave points could be a better marker for LVET assessment. This implies that the true ending of the systolic phase is no longer marked by the dicrotic wave as initially proposed. Hence, in the present study, the aim is to evaluate ET via TDW as depicted in the updated cardiovascular diagram from Figure 1b. More important, the estimation must be tested during different hemodynamic states reflected primarily by the central arterial blood pressure. This method would reveal how strongly LVET estimation is affected by the vasomotor state, and what mitigation measures should be taken for a possible compensation.

2. Methods

2.1. Tidal Wave Terminology

Efficiently evaluating the tidal wave feature for LVET estimation capabilities requires a parametric approach. The starting point for this approach is represented by the first derivative of the signal, as it provides a more detailed view of the blood flow gradient evolution. Based on the visualization and interpretation of various waveform morphologies

from our previous studies [33,34], we have defined the following TDW terminology, as depicted in Figure 2.

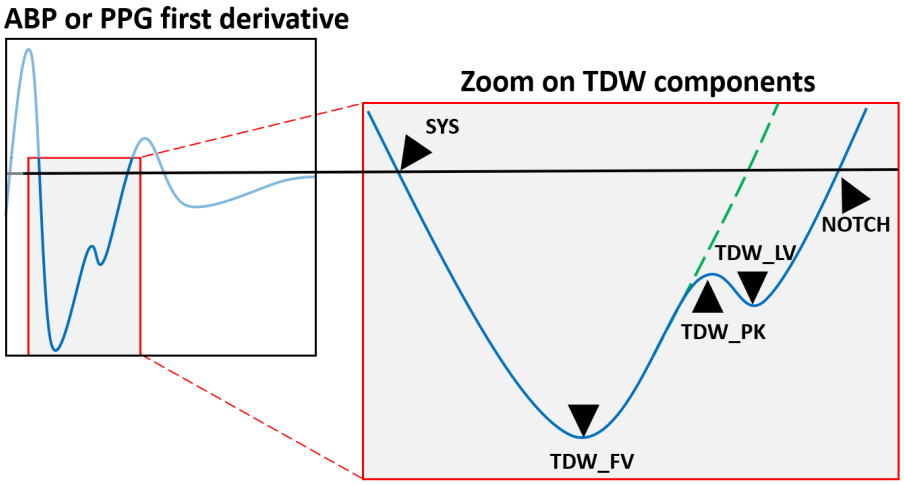


Figure 2. Morphological detail of tidal wave region from first derivative analysis of ABP or PPG waveform. Black line represents zero value. Green dotted line represents gradient convergency to zero value in absence of tidal wave phase. TDW components are highlighted by pointing triangles.

Following the systolic phase, central arterial pressure seeks to return to its initial value, depending on the mechanical resistance encountered in the blood flow. Therefore, when examining the first derivative (FD) domain, the following behavior is observed: after reaching the minimum gradient per cardiac cycle, the trace will eventually converge to a zero value. External or internal stimuli can induce disturbances in blood flow, altering the trajectory of this convergence path. In the context presented here, the onset of aortic valve closure serves as the initial stimulus, leading to the appearance of an inflection point in the gradient trace, labeled as tidal peak (TDW_PK). After the complete closure of the valves, no further disturbances occur, and the convergence trajectory returns to its initial path. This phase creates an additional inflexion point, which is marked as the tidal last valley (TDW_LV). The moment when arterial pressure decay reaches the minimum gradient value just before TDW is labeled as the first valley (TDW_FV).

An essential physiological phenomenon to consider in this context is Windkessel's effect [35,36]. Due to compliant nature of the arterial tree, rapid spikes or changes in flow disturbance are attenuated and prolonged. The elasticity of the blood vessel wall is responsible for this effect, influenced by smooth muscle behavior. When the time constant of compliance capability is shorter than the time duration of a given event, the resulting flow can closely track the change. This is typically observed in predominantly rigid systems. Conversely, when the time constant is longer compared to the disturbance duration, the resulting flow poorly tracks the change. In the human body, this effect, stemming from arterial elasticity, serves to protect vessels' walls from abrupt spikes in blood flow or pressure. Consequently, rapid events are masked both in terms of their amplitude and their time duration. To address this, we introduced a linear compensation fiducial point, TDW_COMP, aimed at reducing Windkessel's effect. For the ABP component, this marker is computed as the midpoint between TDW_PK and TDW_LV. In PPG recordings, the wave propagation time from a central to a peripheral location must be considered. Therefore, the compensation point becomes the midpoint between TDW_FV and TDW_PK.

Regarding the characterization of the dicrotic wave, only one parameter, NOTCH, was considered. This point occurs after the tidal wave's last valley within the FD domain. Thus, measuring notch time duration serves as a spot check to verify the obsolete association with LVET.

2.2. Dataset Acquisition

The open-source database VitalDB [37,38] was employed for LVET assessment in both types of signals: ABP and PPG. A total of up to 6000 individual high-fidelity recordings were gathered from surgical procedures conducted in the operating room. According to the authors, ABP was digitally recorded using Tram-Rac 4A SNUADC, boasting 14-bit resolution and a time resolution of 2 ms (sampling frequency of 500 Hz). For ECG and PPG signals, a Solar 8000 M device with digital storage capability was utilized, maintaining the same sampling frequency. The reference ejection time was measured based on the T-wave segment duration from the ECG signal, as described in the first section. From the clinical data file, an initial selection step was taken regarding patient recordings. The primary inclusion criteria encompassed the following:

- The surgical position was "supine" to eliminate the influence of hydrostatic pressure on the arterial network. This position ensured that all blood vessels were situated on the same horizontal plane and at the same height as the heart.
- The arterial line was placed in the "left radial" position because this vessel is physically closer to the left ventricular location. Consequently, the impact of wave propagation delay is minimized in ABP recordings. However, no information regarding the left or right hand was provided for PPG acquisition.
- The age of the patients was over 20 years old.

After this initial selection, approximately 430 cases met the criteria mentioned above. From this point, the electronic recordings were carefully reviewed by medical experts to ensure they contained readable ECG, ABP and PPG waveforms. Unfortunately, most of the data either had missing ECG waveforms or exhibited distortions in the QRS complex morphology, resulting in only 75 cases remaining for the final analysis. Signal visualization was carried out using MATLAB R2023a software after applying specific processing techniques. The electrocardiogram signal underwent filtering using a 2nd order Butterworth low-pass filter with a cutoff frequency (F3db) of 30 Hz. Similarly, for ABP and PPG waveforms, the same filter was applied, but with a F3bd of 20 Hz. During the signal processing phase, it was observed that a weaker filtering stage more effectively preserved the fiducial points, especially DCW and TDW. Waveform regions were selected from the beginning of case preparation until the surgery began. In the electronic records, the onset of the surgery procedure was marked with a flag. After this point, we lacked additional information regarding surgery stress, except for basic simple numerical readings. Events such blood loss can significantly impact the hemodynamic state, which could strongly influence the results. Therefore, up to this point, only the vasomotor action of the anesthetics drug manifested.

Due to large number of cardiac cycles, artifacts, missing values or waveform morphology deviations were presents. Usually, in the surgery room, these undesired effects occur from touching the patient or the connection plugs of the attached sensors during case preparation. In order to mitigate these inconsistencies, corrupted waveform regions were discarded from the patients' recording. For the artifact elimination procedure, regions were discarded based on medical expertise since certain morphologies cannot occur in the real world. The remaining regions after visual inspection were next analyzed via numerical means. The time duration of the afore-mentioned parameters was computed using an Intellectual Proprietary algorithm. Broadly, the algorithm combines first derivative analysis with logic rule decisions. For every cardiac cycle, it expects the appearance of defined fiducial points with the associated possible locations and also consistency. In this step, clusters of 10 consecutive beats were automatically analyzed via numerical means. This approach helps to mitigate the quasistationary nature of biological signals, which can be attributed to the constant feedback loops within human physiology. One significant biomechanism is the respiratory process, which induces a modulation in both ABP and PPG waveforms as baseline variation [39,40].

Therefore, for each cluster of 10 consecutive beats, the outlier values were discarded by the inbuilt Matlab function *rmoutliers*. The selected method consisted in removing elements more than three standard deviations apart from the mean value. Into the remaining periods

from cluster delimitation, each individual fiducial point result was averaged, by forming a final unique data point. For the interim results, Pearson's correlation factor was used to mitigate possible data anomalies. After the afore-mentioned steps, the final computed data points of each individual patient were merged into a centralized database. No additional discriminating methods were used at this point, apart from artifact and outlier removal.

In the final merged dataset, unique fiducial data points were evaluated again. Even though removing outliers from clusters mitigates results bias, the patients' averaged parameters could represent an outlier value among population evaluation. Again, the same method was used for discarding elements outside the region of three standard deviations. Each computed fiducial point, both from ABP and PPG signals, was subject to this procedure. As long as the resulting point was discarded, the reference linked LVET value was removed too.

Since the data among the population were the most important, additional computation was performed to highlight and discuss the final results. First, the values within one standard deviation (SD) were isolated to underline 68% of the data points. Pearson's correlation coefficients were computed for all resulting data points and for the isolated points. Secondly, a linear regression correlation coefficient was computed only for the one-standard-deviation values. For this step, the *polyval* function in Matlab was used to evaluate the fitted simple regression function, set as a first-order polynomial model. In this way, the trend between the selected fiducial point and the reference LVET was evaluated. Finally, the post-processed dataset among the population, supported by correlation factors, was obtained for results interpretation.

3. Results

During interim processing step, the time duration of the fiducial points was compared to the reference LVET value in individuals, as depicted in Figure 3. These subplots help investigators to detect anomalies of hemodynamic behavior alongside patients' recordings. As shown in subplots (a)–(d), a lack of values appears in the beginning of the recording due to the discarding of corrupted waveforms. Each remaining point represents the average value from ten consecutive beats, after the outliers have been removed. The time duration of TDW_FV, TDW_PK, TDW_LV and NOTCH in both type of signals was measured with respect to the diastolic point, according to Figure 2. The reference value of the ejection time extracted from the ECG was computed as a T-wave segment length.

In Figure 3a,b, the intermediate results are plotted alongside patients' recordings together with the SYS value trend. Here, the trend of the reference LVET value is inversely proportional with the trend of systolic blood pressure. This finding was expected since an increased hemodynamic preload influences cardiac contractility, characterized by a shorter ejection time. Tidal wave components follow the ET trend, but the distance between the associated data points and the reference LVET value is affected by the vasomotor state. On the other hand, the dicrotic component NOTCH overestimates the reference value in both type of waveforms, by having a greater distance between the data points and LVET.

In Figure 3c,d, the LVET estimation error of the selected fiducial points is plotted. Here, it is clearly depicted that the dicrotic notch duration is longer compared to the remaining fiducial point components. For the ABP case, the average value is around 100 ms, while for the PPG case, the result rises to 200 ms. The linear compensation parameter, TDW_COMP, scores a lower error since the corresponding data points are closer to zero values most of the time. The remaining TDW components indicate underestimation and overestimation effects in both types of signals.

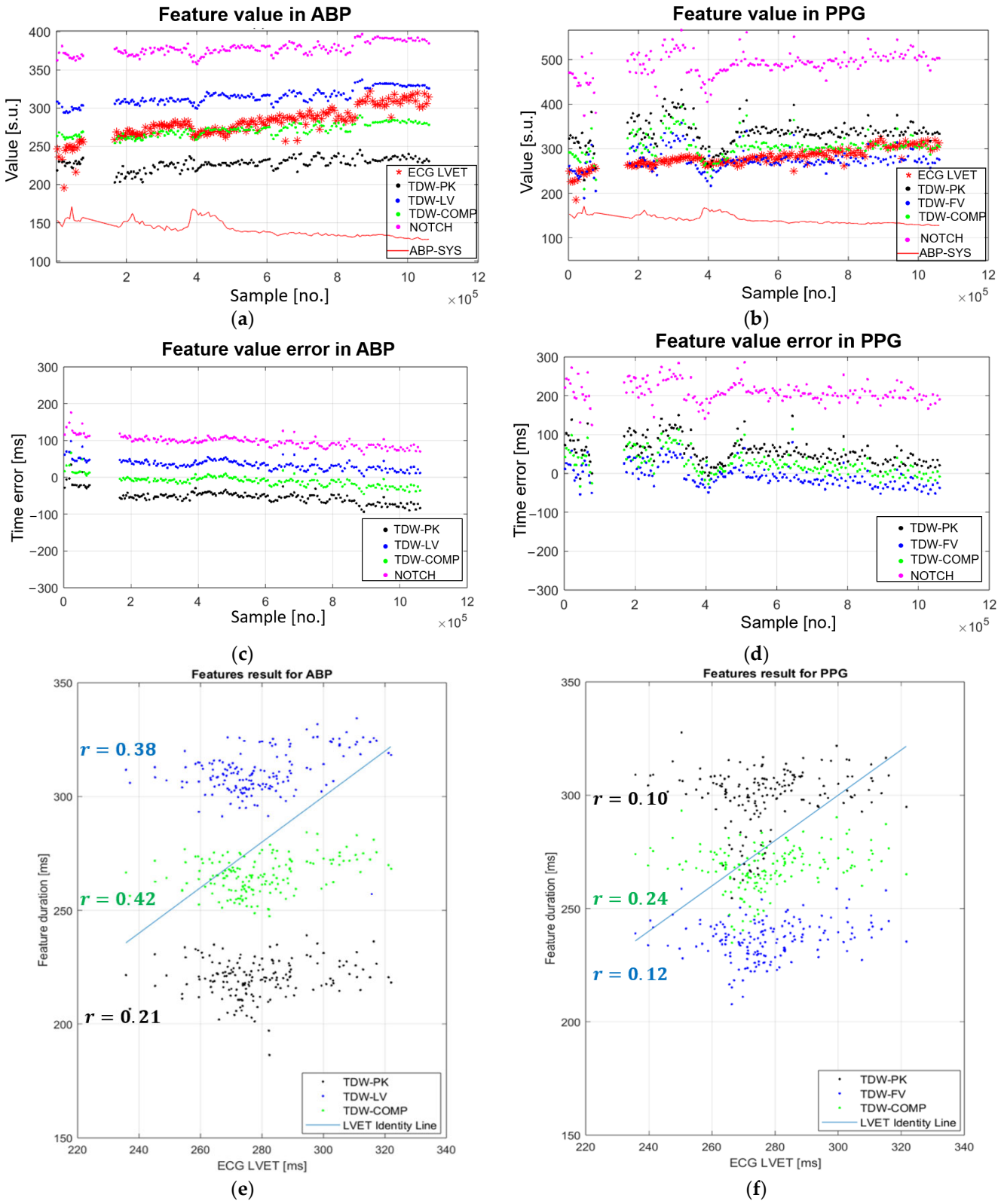


Figure 3. Intermediate results of fiducial points during individual recording evaluation; ID: 0872. Each point represents the average value based on 10 beat cluster evaluation. (**a**,**b**) Feature tracking alongside recording; all units are in milliseconds, except for ABP, which is in in mmHg (s.u.—specific unit); (**c**,**d**) feature error with respect to LVET reference; (**e**,**f**) scatter plot between features and reference LVET.

The last cluster of Figure 3e,f shows the correlation plot between tidal wave components and reference LVET value. In the ABP waveform case, the corresponding TDW_PK data points reflect a shorter time duration than the reference LVET. This finding is linked to the onset of aortic valve closure as was discussed in the terminology section. Therefore, by not reflecting the true onset of the ejection phase, it has a weak Pearson's correlation factor of 0.21. Contrarily, the TDW_LV data points show a longer time duration than the reference value, since Windkessel's effect involves a prolonged propagation time. If, in an ideal case, ABP tracing was recorded near aortic valves, TDW_LV would coincide with the exact moment of valve closure. By moving the measurement site to the peripheral site of the arterial network, TDW_LV is no longer a true match with the real ending phase of ET. The weak agreement between these points is shown by an improved correlation factor of 0.38 compared to the initial one. Hence, the introduction of the compensation point, TDW_COMP, is intended to reduce propagation time delay due to the vascular compliance property. Therefore, this point not only scores a maximum Pearson's correlation factor of 0.42, but also, the data points are closer to the identity line compared to the other TDW components.

For the PPG waveform case, the same trend of the selected fiducial points is present. Due to prolonged delay time in the peripheral site than in the central aortic tree, TDW components contribute in a slightly different manner. As a result, the waveform propagation effect is reflected as reduced correlation coefficients compared to the first case. If in ABP waveform, the TDW_PK data points formed an overestimated result, and in the PPG case, the opposite effect is present. Therefore, in the peripheral site, the true moment of the ejection ending phase occurs before the appearance of the tidal peak component. By evaluating TDW_FV, the obtained data points form a shorter time duration. So, the beginning of the aortic valve closure occurs around this fiducial point location. Again, the same compensation point, TDW_COMP, is computed as the average of the neighborhood signal markers. This parameter scored a maximum Pearson's correlation factor of 0.24. As in the ABP case, the simple linear compensation forms closer data points to the identity line that have a broad intersection region.

On an individual basis, the comparison between ABP and PPG reveals a few findings. First, the measurement site is far away with respect to the heart location, and there is a significant propagation time delay effect. Secondly, the vasomotor state, reflected by arterial blood pressure, changes the compliance factor by affecting Windkessel's effect. An elastic system introduces greater propagation delay time due to mechanical energy absorption. Contrarily, a stiffer network reduces this undesired effect and thus improves the accuracy. This involves an accurate LVET estimation for hypertensive cases, in the absence of any type of result compensation.

Each interim result from the patients' recordings was centralized into the final dataset. The post-processing data from 75 individual recordings amounted to up to 30,000 cardiac cycles. Outliers in the final merged dataset were removed by using the statistic method described in the previous section. After this step, the total beats decreased to 27,000 unique data points. The paired ABP data with the LVET reference value are represented by 15,000 distinctive points and 12,000, respectively, for the PPG case. The remaining data pairs sufficiently cover the ABP spectrum by having a uniform value distribution between 90 and 150 mmHg SYS, as depicted in Figure 4. Since each patient was subject to the anesthesia procedure, the provided ABP readings more frequently show normotensive values rather than hypertensive ones. During intermediate results evaluation, the selection procedure also considered the avoidance of unbalance data points for the afore-mentioned blood pressure classes. At a first glance, balanced data across the entire ABP spectrum reduces the results bias and improves the subsequent interpretation.

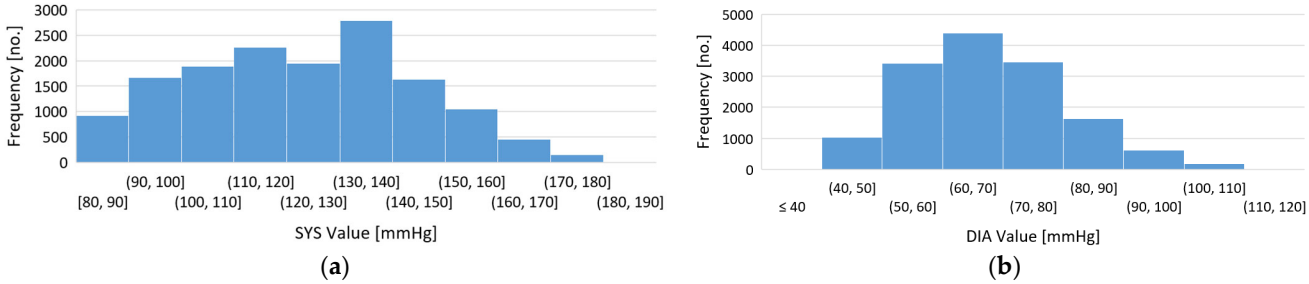


Figure 4. (**a**) Histogram for selected SYS values; (**b**) histogram for selected DIA values.

The final merged results are presented visually on scatter plots (Figure 5) and also supported by numerical values. The NOTCH point is discarded from this step as it is a weak predictor. The results of each individual fiducial point are plotted against the reference LVET for both signals, ABP and PPG. With the blue cross symbol, all the values are shown, while with the red cross symbol, only the values under one standard deviation are highlighted. The last type of data point was computed using a granularity of 20 ms LVET as non-overlapped intervals. Therefore, eight regions are defined in a spectrum of 200 ms to 360 ms. Both types of data points are supported by Pearson's coefficient, *r*, highlighted with the associated color. Additionally, simple linear regression was performed to track the fiducial points values against the reference LVET, as described in the above section. The resulting correlation coefficient is depicted with the R^2 symbol.

For the ABP waveform, the trend of the selected fiducial points is similar to that of the individual case. The first component, TDW_PK, underestimates the true ET, as shown by the isolated SD values. The last tidal wave component, TDW_LV, forms an overestimated result, meaning that the true ET phase has just passed. As a result, this component scores a better Pearson's correlation factor of 0.51, upon analyzing all the data points, than the predecessor tidal peak of 0.39. For the isolated SD values, the *r* parameter increased from 0.47 in TDW_PK to 0.70 in TDW_LV. Upon evaluating the TDW_COMP parameter, the obtained data points have a broad overlapping region over the LVET identity line. Also, this composed fiducial point scores a better Pearson's correlation factor of 0.58 upon analyzing all the data points. The performance of this parameter reached the maximum *r* factor of 0.75 for the isolated SD data points. The rank of the afore-mentioned parameters is also supported by the linear regression coefficient. The compensated point of the tidal wave again obtained the maximum R^2 factor of 0.66.

For the PPG waveform, the consistency of the tidal wave components is inverted, as discussed in the interim results. Due to the waveform propagation effect, from the central aortic tree to the peripheral site, TDW_FV underestimates the reference LVET, as depicted in Figure 5b. On the other hand, TDW_PK overestimates readings in the same manner as the TDW_LV component but from the ABP case. Again, the linear compensation parameter, TDW_COMP, reduces the gap between the data points and the identity line by obtaining the largest overlapping region. This finding is reinforced by the maximum Pearson's correlation factor of 0.53 compared to the previous parameters of 0.49 and 0.50 upon analyzing all data points. For the isolated SD data points, the rank of the fiducial points' relevance is maintained, with a maximum *r* factor of 0.70 for TDW_COMP. Following the evaluation via simple linear regression, the difference between TDW_PK and TDW_COMP is negligible as the R^2 factor increased slightly from 0.47 to 0.49.

Upon comparing the ejection time estimation between ABP and PPG, the compensation parameter is better in the first case, since the signal is recorded from the central part of the arterial network. Therefore, for PPG assessment, more attention is required during the signal processing step to improve LVET accuracy.

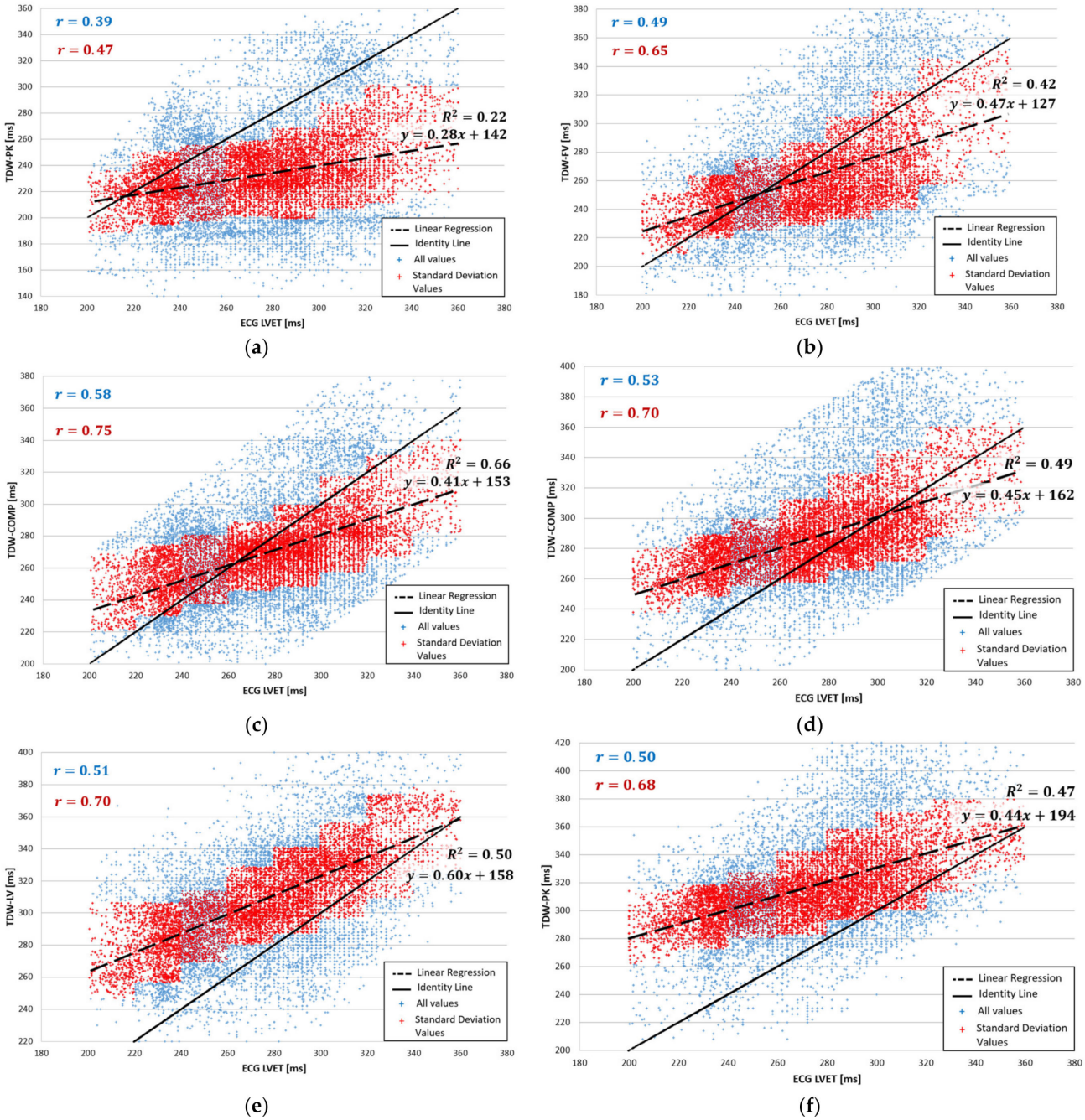


Figure 5. Scatter plot of fiducial point values against LVET reference. On the left side, subfigures (**a**,**c**,**e**) show LVET estimation in ABP signal. On the right side, subfigures (**b**,**d**,**f**) show LVET estimation in PPG signal. Note: in the ABP case, TDW_FV is the first component, while in the PPG case, TDW_PK is the first one according to the terminology section.

The overestimation and underestimation effects of the reference LVET alongside the entire spectrum underline the strong influence of the hemodynamic state among individuals. It is known that a shorter ejection time involves higher cardiac contractility due to an increased preload. In Tables 1 and 2, the defined tidal wave parameters together with the dicrotic notch are compared alongside the ABP spectrum, with a granularity of 10 mmHg.

Table 1. Error values for selected fiducial points in ABP waveform. All results are in milliseconds.

ABP Interval (mmHg)	80–89	90–99	100–109	110–119	120–129	130–139	140–149	150–169	160–169	170+
TDW_PK	-55 ± 21	-57 ± 32	-52 ± 30	-56 ± 33	-59 ± 33	-57 ± 27	-56 ± 30	-54 ± 31	-54 ± 29	-49 ± 23
TDW_LV	-3 ± 24	15 ± 28	18 ± 29	24 ± 26	23 ± 28	28 ± 26	33 ± 23	37 ± 26	38 ± 18	42 ± 17
TDW_COMP	-29 ± 19	-21 ± 24	-17 ± 25	-16 ± 23	-18 ± 25	-14 ± 23	-11 ± 23	-8 ± 25	-8 ± 21	-3 ± 18
NOTCH	61 ± 32	94 ± 34	94 ± 38	96 ± 33	90 ± 38	90 ± 34	100 ± 35	103 ± 34	98 ± 23	99 ± 17

Table 2. Error values for selected fiducial points in PPG waveform. All results are in milliseconds.

ABP Interval (mmHg)	80–89	90–99	100–109	110–119	120–129	130–139	140–149	150–169	160–169	170+
TDW_PK	50 ± 32	51 ± 28	46 ± 33	43 ± 31	41 ± 33	41 ± 34	42 ± 38	30 ± 33	36 ± 31	31 ± 26
TDW_LV	-13 ± 32	-2 ± 31	-7 ± 35	-9 ± 38	-11 ± 38	-14 ± 33	-14 ± 37	-23 ± 36	-9 ± 34	-15 ± 21
TDW_COMP	18 ± 31	25 ± 28	19 ± 32	17 ± 32	15 ± 33	14 ± 32	14 ± 36	4 ± 33	13 ± 31	8 ± 22
NOTCH	154 ± 36	166 ± 41	176 ± 52	186 ± 69	188 ± 70	188 ± 54	195 ± 60	189 ± 58	193 ± 62	167 ± 52

For the ABP case (Table 1), the time difference and standard deviation between the reference LVET and TDW_PK are almost constant. The negative results indicate that the peak appearance happens before the true ending phase of ET. The last tidal wave component, TDW_LV, has a variation between -3 ms and 42 ms, thus indicating that the ET phase has just passed. The compensation point, TDW_COMP, is the most fitted parameter as it shows a maximum absolute error of 29 ms at lower ABP and a minimum absolute error of 3 ms in a higher blood pressure state. The classical NOTCH point shows a strong overestimation between 61 ms and 103 ms; therefore, it is a weak LVET estimator.

For the PPG case (Table 2), the same parametric trend is present as before. The compensation parameter scores a lower absolute error of 25 ms within the lower ABP interval and 4 ms within the higher blood pressure state. The NOTCH parameter is again a weak estimator in the PPG waveform as it obtains an error between 154 ms and 195 ms. In conclusion, TDW components introduce overestimation and underestimation effects, depending on the patient's vasomotor state. These results confirm other findings [29,30] by underlying the importance of vasomotor activity during cardiovascular information extraction.

4. Limitations

Among the presented results, the primary source of error stems from the heterogeneity of the group selected for waveform analysis. The assumption of minimum hemodynamic stress during surgery preparation could be violated in the absence of other additional information. The procedure of anesthetic drug administration, which involves changes in vasomotor activity, could be overlapped with other surgery-related factors that affect the biomechanics of the arterial tree.

Another source of limitation is represented by the large spectrum of waveform morphology variation for ECG, ABP and PPG signals. Even though the medical experts could eliminate corrupted or unreal waveforms, they could not discard small morphology deviations, which are better characterized via numerical means. Due to broad hemodynamic states among the population, various combinations are present between the tidal and dicrotic wave components. Also, during daily activity, users' body movements affect the hemodynamic behavior of the arterial tree, and hence, the morphology of the recorded waveform.

A state-of-the-art automated algorithm could numerically evaluate the obtained morphologies in order to sort between real data and artifacts. The determination of LVET detection is primary affected by prolonged or attenuated fiducial points as a result of Windkessel's effect. This leads to deviations of the waveform gradients from the initially defined path that challenge the algorithm's ability to approximate the true location. Another source of error, observed while running the investigation, implies an additional false change in gradient behavior. This could originate from the compliance property of the

vessel, which induces blood flow oscillation. Since no universal protocol exists for tidal or dicrotic wave components, cardiovascular information extraction cannot be evaluated from a truly objective point of view.

5. Conclusions

An advanced signal processing procedure, especially on the PPG waveform, could extract important cardiovascular markers such LVET. This step considers physical phenomena that occur in the arterial network. The compliance property of blood vessels is characterized by Winkessel's effect, mainly involving a waveform propagation finite time delay alongside an arterial branch. Therefore, the true ending of ET, marked by the ceasing of blood flow disturbance, will be masked both in ABP and PPG signals, as long as physical distance exists between aortic valve location and the measurement site. Since the last waveform type is recorded from the peripheral site, Windkessel's effect will be significant.

A good estimator of LVET in both waveform types is the tidal wave feature, characterized in the first derivative domain by two distinctive points linked to blood pressure disturbance: onset and ending. While this feature is affected by the compliance property of the arterial tree, a linear compensation parameter was computed as the average value between tidal wave components. Even if this new parameter reduces the overestimation and underestimation effects of the true LVET value, the current findings suggest the need for an advanced compensation technique for accuracy improvement.

The dicrotic notch feature has become an obsolete estimator of ET according to both newer findings in the literature and the presented results. Its time location alongside the cardiac cycle is far from the true ET point, with an overestimation over 100 ms. But its amplitude location alongside the ABP or PPG contour reveals information about vasomotor state, as observed in related research [41,42]. This hemodynamic marker could be part of advanced compensation techniques since LVET estimation is strongly dependent on central blood pressure value.

The detection of tidal wave components using the gradient method is critical, mainly for the performance of electronic devices. The ability to record high-quality waveforms is derisible in synergy with advanced signal processing procedures. This need would involve the development of the next generation of wearable devices with improved performance of the PPG technique. Thus, cardiovascular disorders characterized by LVET variation could benefit from remote monitoring with a high confidence level. Also, users or patients would benefit from personalized medicine accessibility. The assessment of extracting valuable cardiovascular information exclusively using PPG technology is a challenging task since waveform morphologies influenced by hemodynamic states are yet to be properly understood.

Another aspect implies a universally agreed measurement protocol for LVET, not only to define a clear prerequisite for assessment but also to develop compensation techniques for an acceptable error range. During a day, a user or patient is subject to uncontrolled settings that render them ineligible for cardiovascular assessment. By defining a clear measurement protocol, ejection time estimation based on non-invasive technology could reach clinical-grade use. The potential applications of this assessment would involve the tracking and monitoring over time of cardiovascular disorders, which are linked to LVET changes such heart failure, hypertension or valvular disease.

Further research will focus on developing advanced compensation techniques in order to improve accuracy. Also, a feasibility study will be conducted to find eligible disorders that could be efficiently tracked via remote LVET measurement.

Author Contributions: Conceptualization, L.E., D.D., S.S. and L.D.; methodology, L.E. and S.S.; software, L.E.; validation, L.E., L.D., S.S. and S.H.; formal analysis, L.E. and S.S.; investigation, L.E.; resources L.E.; data curation, L.E.; writing—original draft preparation, L.E.; writing—review and editing, L.E. and L.D.; visualization. L.E., D.D. and L.D. supervision, L.D. and D.D.; project administration, L.D.; funding acquisition, L.D. All authors have read and agreed to the published version of the manuscript.

Funding: The publication of this paper was funded by the University Politehnica of Bucharest's PUBART project.

Institutional Review Board Statement: Not applicable.

Informed Consent Statement: Not Applicable.

Data Availability Statement: Not Applicable.

Conflicts of Interest: The authors declare no conflict of interest.

References

1. Biering-Sørensen, T.; Querejeta Roca, G.; Hegde, S.M.; Shah, A.M.; Claggett, B.; Mosley, T.H.; Butler, K.R.; Solomon, S.D. Left ventricular ejection time is an independent predictor of incident heart failure in a community-based cohort. *Eur. J. Heart Fail.* **2018**, *20*, 1106–1114. [CrossRef] [PubMed]
2. Alhakak, A.S.; Teerlink, J.R.; Lindenfeld, J.; Böhm, M.; Rosano, G.M.C.; Biering, T. The significance of left ventricular ejection time in heart failure with reduced ejection fraction. *Sørensen Eur. J. Heart Fail.* **2021**, *23*, 541–551. [CrossRef] [PubMed]
3. Altes, A.; Bernard, J.; Dumortier, H.; Dupuis, M.; Toubal, O.; Mahjoub, H.; Jean Tartar, J.; Côté, N.; Clavel, M.A.; O'Connor, K.; et al. Significance of Left Ventricular Ejection Time in Primary Mitral Regurgitation. *Am. J. Cardiol.* **2022**, *178*, 97–105. [CrossRef] [PubMed]
4. Pestelli, G.; Pergola, V.; Totaro, G.; Previtero, M.; Aruta, P.; Cecchetto, A.; Fiorencis, A.; Palermo, C.; Iliceto, S.; Mele, D. Value of Left Ventricular Indexed Ejection Time to Characterize the Severity of Aortic Stenosis. *J. Clin. Med.* **2022**, *11*, 1877. [CrossRef]
5. Iqbal, S.M.A.; Mahgoub, I.; Du, E.; Leavitt, M.A.; Asghar, W. Advances in healthcare wearable devices. *NPJ Flex. Electron.* **2021**, *5*, 9. [CrossRef]
6. Guk, K.; Han, G.; Lim, J.; Jeong, K.; Kang, T.; Lim, E.K.; Jung, J. Evolution of Wearable Devices with Real-Time Disease Monitoring for Personalized Healthcare. *Nanomaterials* **2019**, *9*, 813. [CrossRef]
7. Lee, S.M.; Lee, D. Healthcare wearable devices: An analysis of key factors for continuous use intention. *Serv. Bus.* **2020**, *14*, 503–531. [CrossRef]
8. Lee, H.Y.; Burkard, T. The Advent of Cuffless Mobile Device Blood Pressure Measurement: Remaining Challenges and Pitfalls. *Korean Clin. J.* **2022**, *52*, 198–204. [CrossRef]
9. Falter, M.; Scherrenberg, M.; Driesen, K.; Pieters, Z.; Kaihara, T.; Xu, L.; Caiani, E.G.; Castiglioni, P.; Faini, A.; Parati, G.; et al. Smartwatch-Based Blood Pressure Measurement Demonstrates Insufficient Accuracy. *Front. Cardiovasc. Med.* **2022**, *9*, 958212. [CrossRef]
10. Martínez, G.; Howard, N.; Abbott, D.; Lim, K.; Ward, R.; Elgendi, M. Can Photoplethysmography Replace Arterial Blood Pressure in the Assessment of Blood Pressure? *J. Clin. Med.* **2018**, *7*, 316. [CrossRef]
11. Zadi, A.S.; Alex, R.; Zhang, R.; Watenpaugh, D.E.; Behbehani, K. Arterial blood pressure feature estimation using photoplethysmography. *Comput. Biol. Med.* **2018**, *102*, 104–111. [CrossRef]
12. Chan, G.; Cooper, R.; Hosanee, M.; Welykholowa, K.; Kyriacou, P.A.; Zheng, D.; Allen, J.; Abbott, D.; Lovell, N.H.; Fletcher, R.; et al. Multi-Site Photoplethysmography Technology for Blood Pressure Assessment: Challenges and Recommendations. *J. Clin. Med.* **2019**, *8*, 1827. [CrossRef] [PubMed]
13. Giuseppe, N.; Rosano, A.; Franceschetti, M.E.; Facchetti, P.; Achille, B. Variations in Arterial Blood Pressure and Photoplethysmography During Mechanical Ventilation. *Anesth. Analg.* **2006**, *103*, 1182–1188.
14. Wiggers, C.J. *Modern Aspects of the Circulation in Health and Disease*; Lea & Febiger: Philadelphia, PA, USA, 1923; Chapter VII; p. 98.
15. Mitchell, J.R.; Wang, J. Expanding application of the Wiggers diagram to teach cardiovascular physiology. *Adv. Physiol. Educ.* **2013**, *38*, 170–175. [CrossRef] [PubMed]
16. Tusman, G.; Acosta, C.M.; Pulletz, S.; Böhm, S.H.; Scandurra, A.; Arca, J.M.; Madorno, M.; Sipmann, F.S. Photoplethysmographic characterization of vascular tone mediated changes in arterial pressure: An observational study. *Int. J. Clin. Monit. Comput.* **2018**, *38*, 170–175. [CrossRef] [PubMed]
17. Nirmalan, M.; Dark, P.M. Broader applications of arterial pressure wave form analysis. *Contin. Educ. Anaesth. Crit. Care Pain* **2014**, *14*, 285–290. [CrossRef]
18. Nichols, W.W.; Denardo, S.J.; Wilkinson, I.B.; McEniery, C.M.; Cockcroft, J.; O'Rourke, M.F. Effects of Arterial Stiffness, Pulse Wave Velocity, and Wave Reflections on the Central Aortic Pressure Waveform. *J. Clin. Hypertens.* **2008**, *10*, 295–303. [CrossRef]
19. Mills, J.N. The nature of the limitation of maximal inspiratory and expiratory efforts. *J. Physiol.* **1950**, *111*, 376. [CrossRef]
20. Krovetz, L.J.; Jenningsjr, R.B.; Goldbloom, S.D. Limitation of Correction of Frequency Dependent Artefact in Pressure Recordings Using Harmonic Analysis. *Circulation* **1950**, *50*, 992–997. [CrossRef] [PubMed]
21. Villar, J.; Say, L.; Shennan, A.; Lindheimer, M.; Duley, L.; Conde-Agudelo, A.; Merialdi, M. Methodological and technical issues related to the diagnosis, screening, prevention, and treatment of pre-eclampsia and eclampsia. *J. Gynaecol. Obstet.* **2004**, *85*, S28–S41. [CrossRef] [PubMed]
22. Ponikvar, D. Wilkinson-type ADC with short conversion time and low clock frequency. *Nucl. Instrum. Meth. Phys. Res.* **1998**, *408*, 523–529. [CrossRef]
23. Luisada, A.A.; MacCanon, D.M. The phases of the cardiac cycle. *Am. Heart J.* **1972**, *83*, 705–711. [CrossRef]
24. Yu, C.M.; Sanderson, J.E.; Marwick, T.H.; Oh, J.K. Tissue Doppler Imaging: A New Prognosticator for Cardiovascular Diseases. *J. Am. Coll. Cardiol.* **2007**, *49*, 1903–1914. [CrossRef]

25. Nikitin, N.P.; Witte, K.K.A. Application of Tissue Doppler Imaging in Cardiology. *Cardiology* **2004**, *101*, 170–184. [CrossRef]
26. Pricea, D.J.A.; Wallbridgeb, D.R.; Stewarta, M.J. Tissue Doppler imaging: Current and potential clinical applications. *Heart* **2000**, *84*, ii11–ii18. [CrossRef] [PubMed]
27. Anavekar, S.N.; Oh, K.J. Doppler echocardiography: A contemporary review. *J. Cardiol.* **2009**, *54*, 347–358. [CrossRef] [PubMed]
28. Chan, G.S.H.; Middleton, P.M.; Celler, B.G.; Wang, L.; Lovell, N.H. Automatic detection of left ventricular ejection time from a finger photoplethysmographic pulse oximetry waveform: Comparison with Doppler aortic measurement. *Physiol. Meas.* **2007**, *28*, 439–452. [CrossRef] [PubMed]
29. Obata, Y.; Mizogami, M.; Singh, S.; Nyhan, D.; Berkowitz, D.E.; Steppan, J.; Barodka, V. Ejection time: Influence of hemodynamics and site of measurement in the arterial tree. *Hypertens. Res.* **2017**, *40*, 811–818. [CrossRef]
30. Middleton, P.M.; Chan, G.S.H.; O'Lone, E.; Steel, E.; Carroll, R.; Celler, B.G.; Lovell, N.H. Changes in left ventricular ejection time and pulse transit time derived from finger photoplethysmogram and electrocardiogram during moderate haemorrhage. *Clin. Physiol. Funct. Imaging* **2009**, *29*, 163–169. [CrossRef]
31. Aase, S.A.; Torp, H.; Støylen, A. Aortic valve closure: Relation to tissue velocities by Doppler and speckle tracking in normal subjects. *Eur. J. Echocardiogr.* **2008**, *9*, 555–559. [CrossRef]
32. Finnegan, E.; Davidson, S.; Harford, M.; Watkinson, P.; Tarassenko, L.; Villarroel, M. Features from the photoplethysmogram and the electrocardiogram for estimating changes in blood pressure. *Sci. Rep.* **2023**, *13*, 986. [CrossRef]
33. Evdochim, L.; Zhdanov, A.E.; Dobrescu, L.; Dobrescu, D.; Dolganov, A.Y. Blood Pressure and Photoplethysmography Waveform Classification by Signal's Morphology. In Proceedings of the Ural-Siberian Conference on Biomedical Engineering, Radioelectronics and Information Technology (USBEREIT), Yekaterinburg, Russia, 19–21 September 2022.
34. Evdochim, L.; Dobrescu, D.; Halichidis, S.; Dobrescu, L.; Stanciu, S. Hypertension Detection Based on Photoplethysmography Signal Morphology and Machine Learning Techniques. *Appl. Sci.* **2022**, *12*, 8380. [CrossRef]
35. Belz, G.G. Elastic properties and Windkessel function of the human aorta. *Cardiovasc. Drugs Ther.* **1995**, *9*, 73–83. [CrossRef] [PubMed]
36. Westerhof, N.; Lankhaar, J.W.; Westerhof, B.E. The arterial Windkessel. *Med. Biol. Eng. Comput.* **2009**, *47*, 131–141. [CrossRef]
37. Lee, H.C.; Jung, C.W. Vital Recorder—A free research tool for automatic recording of high-resolution time-synchronised physiological data from multiple anaesthesia devices. *Sci. Rep.* **2018**, *8*, 1527. [CrossRef] [PubMed]
38. Lee, H.C.; Park, Y.; Yoon, S.B.; Yang, S.M.; Park, D.; Jung, C.W. VitalDB, a high-fidelity multi-parameter vital signs database in surgical patients. *Sci. Data* **2022**, *9*, 279. [CrossRef]
39. Hayano, J.; Yasuma, F.; Okada, A.; Mukai, S.; Fujinami, T. A Phenomenon Improving Pulmonary Gas Exchange and Circulatory Efficiency. *Circulation* **1996**, *94*, 842–847. [CrossRef] [PubMed]
40. Baker, S.; Xiang, W.; Atkinson, I. Determining respiratory rate from photoplethysmogram and electrocardiogram signals using respiratory quality indices and neural networks. *PLoS ONE* **2021**, *16*, e0249843. [CrossRef] [PubMed]
41. Hébert, J.L.; Lecarpentier, Y.; Zamani, K.; Coirault, C.; Daccache, G.; Chemla, D. Relation between aortic dicrotic notch pressure and mean aortic pressure in adults. *Am. J. Cardiol.* **1995**, *76*, 301–306. [CrossRef] [PubMed]
42. Joachim, J.; Coutrot, M.; Millasseau, S.; Matéo, J.; Mebazaa, A.; Gayat, E.; Vallée, F. Real-time estimation of mean arterial blood pressure based on photoplethysmography dicrotic notch and perfusion index. A pilot study. *J. Clin. Monit. Comput.* **2020**, *35*, 395–404. [CrossRef] [PubMed]

Disclaimer/Publisher's Note: The statements, opinions and data contained in all publications are solely those of the individual author(s) and contributor(s) and not of MDPI and/or the editor(s). MDPI and/or the editor(s) disclaim responsibility for any injury to people or property resulting from any ideas, methods, instructions or products referred to in the content.